Neurobiology of Learning and Memory 129 (2016) 38–49

Contents lists available at ScienceDirect

Neurobiology of Learning and Memory

journal homepage: www.elsevier.com/locate/ynlme

Review

# Tracking the flow of hippocampal computation: Pattern separation, pattern completion, and attractor dynamics

James J. Knierim [a,*], Joshua P. Neunuebel [b]

[a] Krieger Mind/Brain Institute and Solomon H. Snyder Department of Neuroscience, Johns Hopkins University, United States
[b] Dept. of Psychological and Brain Sciences, University of Delaware, United States

ARTICLE INFO

*Article history:*
Received 7 June 2015
Revised 4 October 2015
Accepted 21 October 2015
Available online 26 October 2015

*Keywords:*
Place cells
Attractors
Pattern completion
Pattern separation
Dentate gyrus
CA3

ABSTRACT

Classic computational theories of the mnemonic functions of the hippocampus ascribe the processes of pattern separation to the dentate gyrus (DG) and pattern completion to the CA3 region. Until the last decade, the large majority of single-unit studies of the hippocampus in behaving animals were from the CA1 region. The lack of data from the DG, CA3, and the entorhinal inputs to the hippocampus severely hampered the ability to test these theories with neurophysiological techniques. The past ten years have seen a major increase in the recordings from the CA3 region and the medial entorhinal cortex (MEC), with an increasing (but still limited) number of experiments from the lateral entorhinal cortex (LEC) and DG. This paper reviews a series of studies in a local–global cue mismatch (double-rotation) experiment in which recordings were made from cells in the anterior thalamus, MEC, LEC, DG, CA3, and CA1 regions. Compared to the standard cue environment, the change in the DG representation of the cue-mismatch environment was greater than the changes in its entorhinal inputs, providing support for the theory of pattern separation in the DG. In contrast, the change in the CA3 representation of the cue-mismatch environment was less than the changes in its entorhinal and DG inputs, providing support for a pattern completion/error correction function of CA3. The results are interpreted in terms of continuous attractor network models of the hippocampus and the relationship of these models to pattern separation and pattern completion theories. Whereas DG may perform an automatic pattern separation function, the attractor dynamics of CA3 allow it to perform a pattern separation or pattern completion function, depending on the nature of its inputs and the relative strength of the internal attractor dynamics.



## 1. Introduction

Although most computational theories of the mnemonic functions of the hippocampus have focused on the CA3 and dentate gyrus (DG) regions, the large majority of single-unit studies of the hippocampus have been recordings from the CA1 region. This emphasis on CA1 is understandable for both functional and practical reasons. CA1 is the region that primarily transmits the output of DG/CA3 processing to the rest of the cerebrum (Witter & Amaral, 2004). Thus, it can serve as a functional readout of the information provided by the hippocampus to other brain areas that are involved in hippocampus-dependent cognition and behavior. Moreover, CA1 is the first cell layer encountered in the rodent hippocampus when an electrode is advanced from the dorsal surface of the brain, and it is by far the easiest layer of the hippocampus to record large ensembles of well-isolated units.

Although recordings from CA1 can illuminate the types of information and representations being sent to other brain regions, these recordings in isolation can inform little about the nature of the information processing that occurs within the hippocampal circuitry. For example, one may know that CA1 place cells form independent spatial representations of two distinct environments (Bostock, Muller, & Kubie, 1991). However, this knowledge alone tells us little about the computational processing that creates these two representations, and whether that processing occurs within CA1, in upstream hippocampal regions like DG or CA3, or even in regions entirely afferent to the hippocampus. To understand the neural computations of the hippocampus, it is necessary to understand the information represented in hippocampal inputs, in its internal processing stages, and in its outputs, as well as the transformations that occur as information is processed through these circuits.

* Corresponding author at: Krieger Mind/Brain Institute, Johns Hopkins University, 338 Krieger Hall, 3400 N. Charles Street, Baltimore, MD 21218, United States. Fax: +1 410 516 8648.
*E-mail address:* jknierim@jhu.edu (J.J. Knierim).

http://dx.doi.org/10.1016/j.nlm.2015.10.008
1074-7427/

This article will review a series of studies from our lab over the past decade in which we recorded the activity of hippocampal input regions and output regions, as well as the intrahippocampal processing in the DG and CA3 regions. To induce controlled, parametric changes to the animal's environment, we used a "double rotation" manipulation, in which the local reference frame of the behavioral track was placed in varying degrees of conflict with the global reference frame of the laboratory environment (Knierim, 2002; Shapiro, Tanila, & Eichenbaum, 1997). We investigated how neural populations in the hippocampal system responded to these alterations in order to deduce the neural representations and computations associated with the different regions. In particular, we addressed the questions of whether we can interpret (1) DG responses as evidence for its proposed role of performing pattern separation on its inputs and (2) CA3 responses as evidence for its proposed role of performing pattern completion (or the related concepts of error correction and generalization) on its inputs. We begin with a brief history of the computational theories of pattern separation and completion.

## 2. Classic theories of DG function: Pattern separation in DG vs. pattern completion in CA3

The most prominent theory of DG function is the pattern separation theory (Kesner, Gilbert, & Wallenstein, 2000; McNaughton & Morris, 1987; McNaughton & Nadel, 1990; Rolls & Treves, 1998; Yassa & Stark, 2011), which originated in David Marr's theory of the cerebellum (Marr, 1969). Marr proposed that the cerebellar granule layer created a very sparse representation of incoming sensorimotor input by an *expansion recoding* strategy; that is, highly overlapping representations encoded by populations of pontine mossy fibers, which formed synapses onto an enormous layer of cerebellar granule cells, were transformed into extremely sparse, independent representations in the granule layer. This transformation allowed the storage, with minimal interference, of the countless contexts in which a movement occurred. Investigators elaborated Marr's subsequent theory of the hippocampus (Marr, 1971) and ascribed a similar function to the DG granule cell layer (McNaughton & Morris, 1987; McNaughton & Nadel, 1990; Myers & Scharfman, 2009, 2011; O'Reilly and McClelland, 1994; Rolls & Treves, 1998). If the entorhinal cortex (EC) represented two experiences with a high degree of overlap in the population of active cells, an expansion recoding mechanism caused the hippocampal granule layer to create representations that overlapped considerably less than its EC inputs. This process is illustrated in Fig. 1, which shows a hypothetical relationship between two input patterns and two output patterns. Each sphere represents a cell in the population, and the colored spheres represent the currently active neurons. The input patterns show great overlap, in that each pattern shares 2 of the 3 active neurons. With expansion recoding onto a larger output population, there is no overlap in the sets of active cells.

Pattern separation may be graphically illustrated in terms of the input–output curves of the DG (Fig. 2A). Consider how the DG and the EC represent two different events. The *x*-axis represents the difference in the combined medial entorhinal cortex (MEC) and lateral entorhinal cortex (LEC) representations of the two events. This difference may be quantified by the correlation of neural population activity between the representations of each event (a high Δinput corresponds to a low correlation between the two representations). The *y*-axis represents the difference in the corresponding DG representations. According to the pattern separation theory, the Δoutput of the DG is greater than the Δinput from the EC, quickly reaching a maximum difference (i.e., the DG representations of the two experiences are completely decorrelated, even when the Δinput is still fairly small). In support of the theory that the DG performs such an operation, rats with selective DG lesions were impaired in tasks thought to rely on spatial pattern separation (Gilbert, Kesner, & Lee, 2001); genetic knockout of the NR1 subunit of the NMDA receptor in DG impaired the ability of mice to discriminate similar environments in a fear conditioning experiment (McHugh et al., 2007); and CA3 place fields in these mice were impaired in the discrimination of two environments (McHugh et al., 2007). Human imaging studies have supported a role of the hippocampus in pattern separation, but these studies were limited by an inability to resolve the DG and CA3 regions (Bakker, Kirwan, Miller, & Stark, 2008). (For more detailed reviews, see Rolls & Kesner, 2006; Santoro, 2013; Yassa & Stark, 2011.)

The complementary role of pattern completion is commonly ascribed to the CA3 region. Strictly defined, pattern completion refers to the ability of a network to retrieve from memory a complete pattern of activity when presented with incomplete or degraded input patterns; for example, a network may output a complete phone number when presented with only a fraction of the number as a retrieval cue. This process is thought to be the result of the recurrent collateral circuitry providing an anatomical basis for an autoassociative network, that is, a network in which activity patterns can become associated with themselves. Such a network might also display attractor dynamics. In general terms, an attractor refers to a set of stable states in a system that have the property that they "attract" neighboring states to move toward the stable states, like a magnet attracts nearby metal particles or like a ball rolls down the slope of a hill toward a valley (Knierim & Zhang, 2012). Attractor dynamics in CA3, in concert with pattern

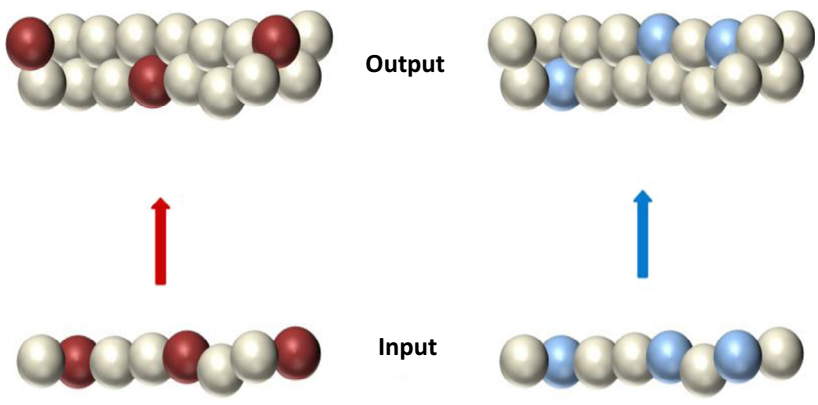


**Fig. 1.** Pattern separation by expansion recoding. Input patterns (colored cells) at bottom overlap more than the output patterns at top. (For interpretation of the references to colour in this figure legend, the reader is referred to the web version of this article.)

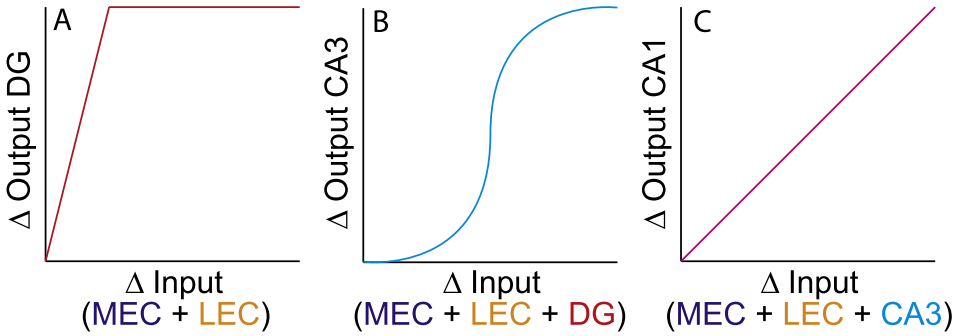


**Fig. 2.** Hypothesized input–output curves for the DG, CA3, and CA1 regions of the hippocampus. The *x*-axis of each graph denotes the difference between the neural activity representations of two specific input patterns. The *y*-axis represents the difference between the corresponding output patterns. (A) The DG is hypothesized to change its output patterns to a greater extent than the input patterns change (pattern separation). (B) CA3 is hypothesized to show a sigmoidal relationship between Δinput and Δoutput, performing pattern completion with small Δinput and pattern separation with large Δinput. (C) CA1 is hypothesized to display a linear relationship between Δinput and Δoutput.

separation processing in its DG inputs, may cause the CA3 network to display outputs that show both pattern separation and pattern completion.

Fig. 2B shows the sigmoidal relationship between pattern input similarity (from combined MEC, LEC, and DG inputs) and pattern output similarity that arises from these attractor dynamics (Guzowski, Knierim, & Moser, 2004; McClelland & Goddard, 1996; Rolls & Treves, 1998). When two input representations are similar (Δinput ≈ 0), the output representations are also very similar (Δoutput ≈ 0). As the representations diverge (Δinput > 0, but still small), the output representations of CA3 maintain a higher degree of similarity than the inputs (Δoutput < Δinput). This resistance to changes in the input is caused by the putative attractor dynamics of CA3 (Knierim & Zhang, 2012). The inputs cause CA3 cells to fire within the basin of attraction set up by the rat's previous experiences. The attractor dynamics cause the CA3 representation to move closer to the Δoutput ≈ 0 state, although the influences from the external input prevent the two representations from being completely correlated (i.e., Δoutput > 0). As the Δinput increases further, eventually the attractor dynamics cause a nonlinear change in the Δoutput, causing the output representations to be less similar than the inputs (pattern separation: Δoutput > Δinput). This can be interpreted as the input representations of each experience causing the CA3 representations to fall into two distinct attractor states that are mutually inhibited.

Note that the recurrent collaterals and putative attractor dynamics of CA3 do not just reflect pattern completion. When Δinput is small, CA3 reflects pattern completion (Δoutput < Δinput). When Δinput is large, CA3 output reflects pattern separation (Δoutput > Δinput). Note also that in this model, pattern completion, error correction, and generalization are all different instances of the same underlying computational dynamics. Outputs can be made more similar than the inputs when the changes to the input (Δinput) are due to missing or degraded parts of the representation (pattern completion), small errors in the input representation (error correction), or small differences in the representations of legitimately similar inputs (generalization). Although these different cases might result in variations in the shape of the sigmoid (e.g., making it shallower or sharper; moving the inflection point along the *x* axis), the attractor dynamics will endow the CA3 with qualitatively similar, nonlinear, input–output curves. Thus, rather than performing pattern separation *per se*, the CA3 output can be thought of as the final arbiter between the pattern separation processes of the DG inputs and the pattern completion processes of the recurrent collateral circuitry.

Fig. 2C shows the hypothesized relationship between input changes and output changes for CA1 (Guzowski et al., 2004). Lacking both the numerical expansion between the input and output layers of DG and the strong, recurrent collateral system of CA3, CA1 is thought to show a more linear relationship between its inputs and outputs (as Δinput increases, Δoutput increases by approximately the same amount). Note that this linear relationship does not predict that CA1 will necessarily vary its inputs in linear proportion to changes in the external environment or other experimental manipulations. The Δinput to CA1 includes not only the entorhinal representations, but also the input from CA3. Thus, CA1 might show nonlinear changes in its place cell outputs as a function of experimental manipulations, but this might reflect nonlinear changes inherited from CA3, rather than nonlinear processing in CA1 itself. In other words, if one could measure precisely the changes in the CA1 inputs and the changes in the CA1 outputs, the input–output curve might show a linear change as in Fig 2C, even if the output of CA1 plotted relative to changes in the experimental manipulations is highly nonlinear.

## 3. Double rotation experiments

With these considerations in mind, we will now review a series of neurophysiological recording experiments from hippocampal afferent regions (the MEC, LEC, and anterior thalamus), intrahippocampal regions (DG and CA3), and the hippocampal output layer (CA1). In these experiments, rats ran clockwise on a circular track (Knierim, 2002) (Fig. 3). The track was divided into 4 quadrants, each with a distinct visual and tactile texture. The track was centered in a room with a circular, black curtain at the periphery. Along the curtain were 6 salient global cues. After many days of training to run laps on the track for irregularly placed food reward, the rats experienced over 4 days a sequence of alternating sessions in which the cues were arranged in the standard configuration (standard session) or in a mismatched configuration (mismatch session). The mismatches were generated by rotating the local cues on the track in a counterclockwise (CCW) direction and the cues along the curtains by an equal amount in a clockwise (CW) direction (double rotation). The net mismatch between the local and global reference frames was 45°, 90°, 135°, or 180°.

### *3.1. Superficial-layer MEC spatial representations and thalamic head direction representations are controlled by the global cues*

The superficial layers of MEC provide the major spatial information to the hippocampus, in the form of grid cells, boundary cells, and head direction cells (Hafting, Fyhn, Molden, Moser, & Moser, 2005; Sargolini et al., 2006; Savelli, Yoganarasimha, & Knierim, 2008; Solstad, Boccara, Kropff, Moser, & Moser, 2008; Zhang

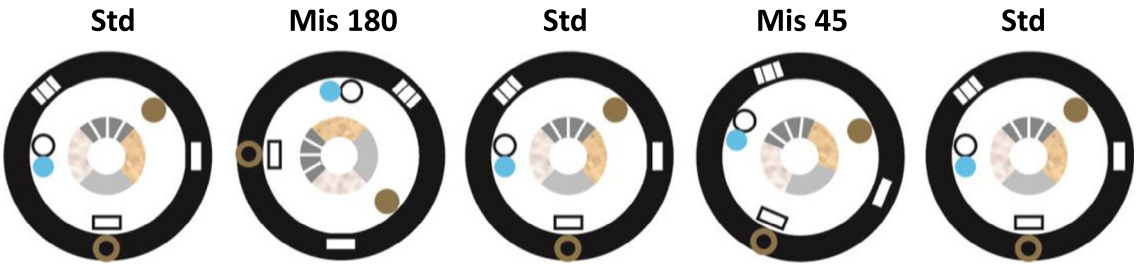


**Fig. 3.** Double rotation experiment. The inner circle denotes the behavioral track with different local textures on the 4 quadrants. The black, outer ring denotes the circular curtain at the perimeter, with 6 distinct landmarks that constitute the global cue set. Shown here is a typical sequence of recordings, with 3 standard sessions interleaved with 2 mismatch sessions (180° and 45°). In the mismatch sessions, the local cues are rotated CCW and the global cues are rotated CW by the same amount. From Neunuebel et al. (2013).

et al., 2013). MEC cells are modulated by the theta rhythm, just like place cells (Brun et al., 2008; Hafting, Fyhn, Bonnevie, Moser, & Moser, 2008; Ranck, 1973; Stewart, Quirk, Barry, & Fox, 1992). MEC cells, CA1 place cells, and head direction cells appear to be tightly coupled to each other: When head direction cells rotate their preferred firing directions in an environment, both MEC cells and place cells rotate their spatial tuning profiles by equal amounts (Hargreaves, Yoganarasimha, & Knierim, 2007; Knierim, Kudrimoti, & McNaughton, 1995, 1998). Under most circumstances, head direction cells are controlled by the most peripheral landmarks in an environment (Taube, Muller, & Ranck, 1990; Zugaro, Berthoz, & Wiener, 2001). Thus, as predicted, head direction cells of the thalamus changed their preferred firing directions to follow the global cues in the double rotation experiment (Fig. 4). Whenever more than one head direction cell was recorded simultaneously (range 2–7 cells), all of the head direction cells rotated by the same amount. This result provided convincing evidence that the head direction system formed a tightly coupled network, consistent with ring attractor models of head direction cells (see below for further descriptions of ring attractors) (Skaggs, Knierim, Kudrimoti, & McNaughton, 1995; Zhang, 1996; Blair, 1996; Redish, Elga, & Touretzky, 1996; Song & Wang, 2005; Knierim & Zhang, 2012).

Because of the close anatomical association between areas with head direction cells and the MEC (Witter & Amaral, 2004), along with the presence of head direction cells in MEC (Sargolini et al., 2006) and the previously described coupling between head direction cells and MEC spatial firing (Hargreaves et al., 2007), one would predict that the MEC spatial representations would be controlled strongly by the global cues in the mismatch sessions. As predicted, the firing fields of MEC cells rotated in alignment with the global cues (Neunuebel, Yoganarasimha, Rao, & Knierim, 2013). Fig. 5A shows population correlation matrices between two standard sessions (left) and between a standard and mismatch session (right). Each pixel in the matrix represents the correlation between the population vectors representing the location of the rat (in degrees of angle along the track) in one session and the next. The band of high correlation (bright white stripe) along the main diagonal on the left matrix indicates that the MEC population representation of location was stable between the two standard sessions (i.e., the population vector was highly correlated between the same locations on the track in the two sessions and poorly correlated between different locations). During the mismatch session (right), the correlation band was maintained, but shifted above the main diagonal (red dashed line), indicating that the representations followed the rotation of the global cues in the mismatch session. We converted the 2-dimensional correlation matrices into 1-dimensinal polar plots by calculating the average correlation of all pixels along the diagonals of the matrix (Fig. 5B). Fig. 5C shows a well-formed tuning curve for the STD1–STD2 correlation (gray) and a similarly well-formed tuning curve for the STD1-MISMATCH correlation (purple), rotated 45° clockwise to follow the global cue set.

The responses to all mismatch angles are represented as polar plots in Fig. 6A. As the cue-mismatch increased in magnitude, the population correlations between the standard and mismatch ses-

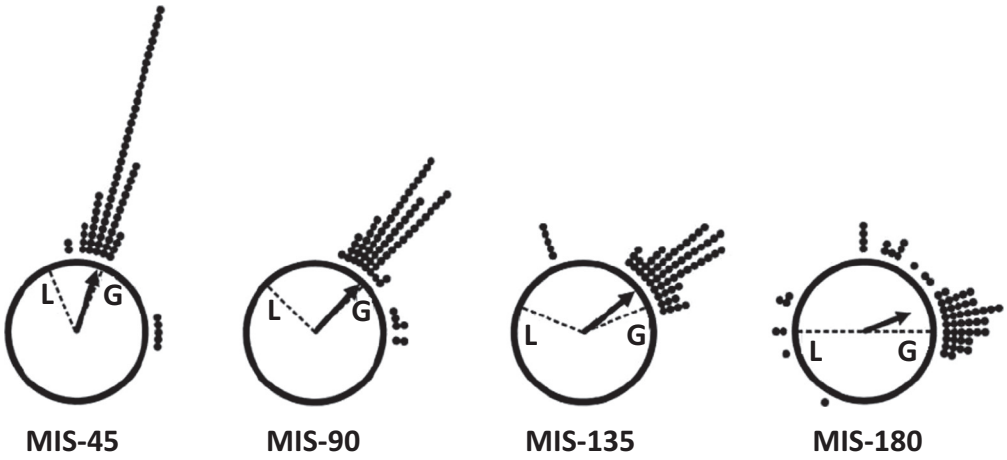


**Fig. 4.** Head direction cell responses to the double rotation. In these circular histograms, 0° is at the top of the plot. Each dot indicates the rotation angle of the directional tuning curve of a head direction cell between the standard session and a mismatch session. For example, if the preferred direction of a cell rotated 90° between sessions, a dot is added to the circle corresponding to 90° (i.e., at the 3 o'clock position) "L" indicates the rotation of the local cues and "G" indicates the rotation of the global cues. Almost all head direction cells rotated by approximately the same amount as the global cues. Modified from Yoganarasimha, Yu, and Knierim (2006).

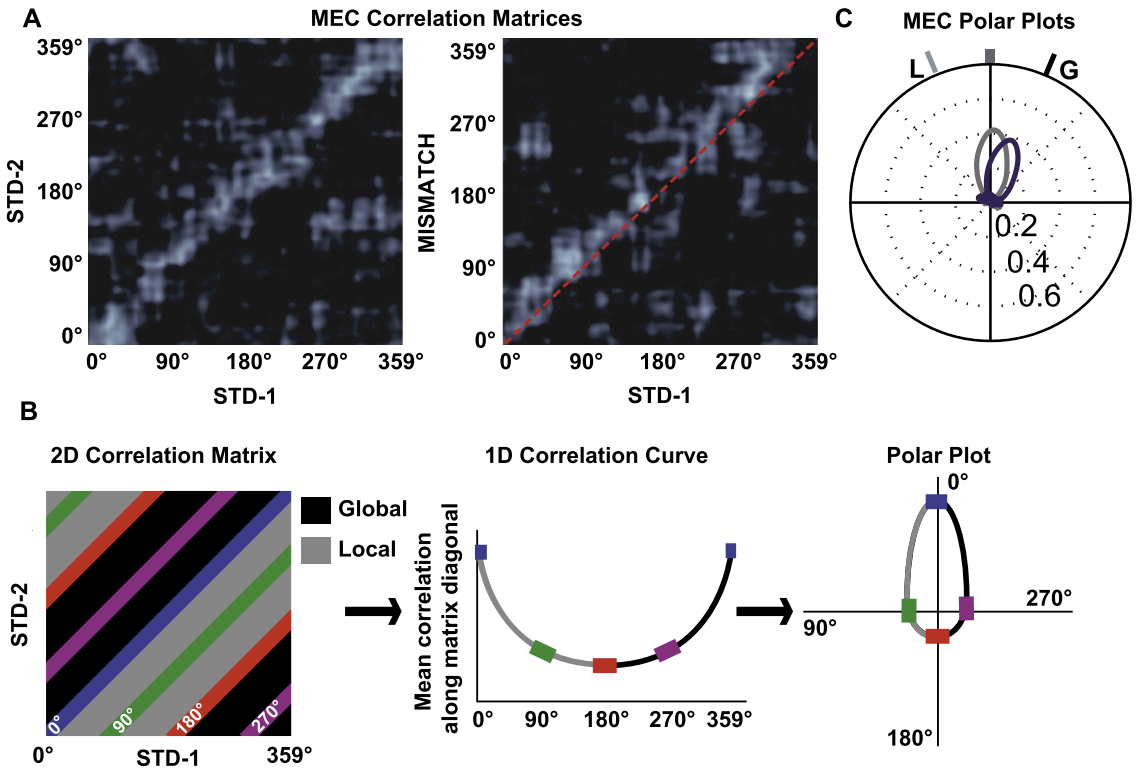


**Fig. 5.** Conversion of 2-dimensional population correlation matrices to 1-dimensional polar plots. (A) MEC population correlation matrices were calculated for two standard sessions (STD-1 vs. STD-2, left) and for a standard-mismatch session (STD-1 vs. MISMATCH, right). The *x*- and *y*-axes of the plots indicate the location of the rat on the circular track binned in 1° increments from 0 to 359. Each bin of the 360 × 360 matrix shows the correlation between the MEC population vectors of neural activity when the rat is located at the corresponding bin of the two track sessions. The band of high correlation (white) along the main diagonal of the STD-1 vs. STD-2 matrix shows that spatial representation of the MEC population was stable between the two sessions. A similar band is seen on the STD-1 vs. MISMATCH matrix, but the band is shifted upward relative to the main diagonal (dashed line), indicating that the representation rotated coherently in the MISMATCH session along with the global cues. (B) To transform the correlation matrix into a polar plot, the correlations of all the pixels along each diagonal of the matrix are averaged, generating a 1-dimensional line graph. The line graph is then transformed into a polar plot, with the mean correlation plotted on the radial axis and the angle of rotation plotted as an angular coordinate. (C) The polar plot representations of the two correlation matrices from part A are shown, with the STD-1 vs. STD-2 plot in gray and the STD-1 vs. MISMATCH plot in purple. L indicates the rotation of the local cues and G indicates the rotation of the global cues. Modified from Neunuebel et al. (2013). (For interpretation of the references to colour in this figure legend, the reader is referred to the web version of this article.)

sions decreased, indicating that the MEC representations continuously degraded with increasing local–global conflict. This decorrelation may reflect a combination of CW rotations of the underlying grid cells and other spatial cells (following the global cue set) as well as potential shifts of the grid in the horizontal plane, as the representations become decoupled from the external landmarks in the environment. In general, though, the MEC representations followed the global cues, with little evidence of a strong, local-cue driven component to the MEC population response.

### 3.2. Superficial-layer LEC representation is controlled by the local cues

In contrast to the MEC, grid cells and head direction cells appear to be absent in LEC (Hargreaves, Rao, Lee, & Knierim, 2005; Knierim, Neunuebel, & Deshmukh, 2013; Yoganarasimha, Rao, & Knierim, 2011), and LEC cells are much more weakly modulated by theta compared to MEC and hippocampal cells (Deshmukh, Yoganarasimha, Voicu, & Knierim, 2010). Superficial-layer LEC cells fire in the presence of discrete objects in an environment, and under these conditions a small minority show spatial tuning profiles that resemble the robust place fields of the hippocampus, even when the firing location is away from the objects (Deshmukh & Knierim, 2011). Thus, one might predict that LEC cells would be more strongly controlled by local cues on the track, rather than the global landmarks on the curtains. Consistent with this prediction, Neunuebel et al. (2013) demonstrated that, even though the LEC did not have a robust spatial representation of the track, there was a significant correlation between the LEC representations of the standard and mismatch sessions, and this representation was clearly controlled by the local cues (Fig. 6B). (Note that we only analyzed firing when the rat's head was on the track and the rat was moving forward at a minimal speed. We did not analyze neural activity when the rat was looking off the track, performing so-called "head scanning" behavior and potentially attending to individual cues on the curtains (Monaco, Rao, Roth, & Knierim, 2014)).

### 3.3. DG performs pattern separation on its EC inputs

Given that the MEC and LEC are the major inputs to the DG, we can begin to measure the Δinput–Δoutput curve of the DG (Neunuebel & Knierim, 2014). As the cue mismatch increased, the MEC representation gradually degraded (Δinput increased) and was controlled by the global cues (Fig. 6A). In contrast, the LEC representation was not strongly correlated between the standard and mismatch sessions for any cue-mismatch angle, but a weak, local-cue-controlled signal was detectable (Fig. 6B). The DG representation of the 45° mismatch environment was very similar to the standard environment, as the two representations were highly correlated (although less correlated than the standard ses-

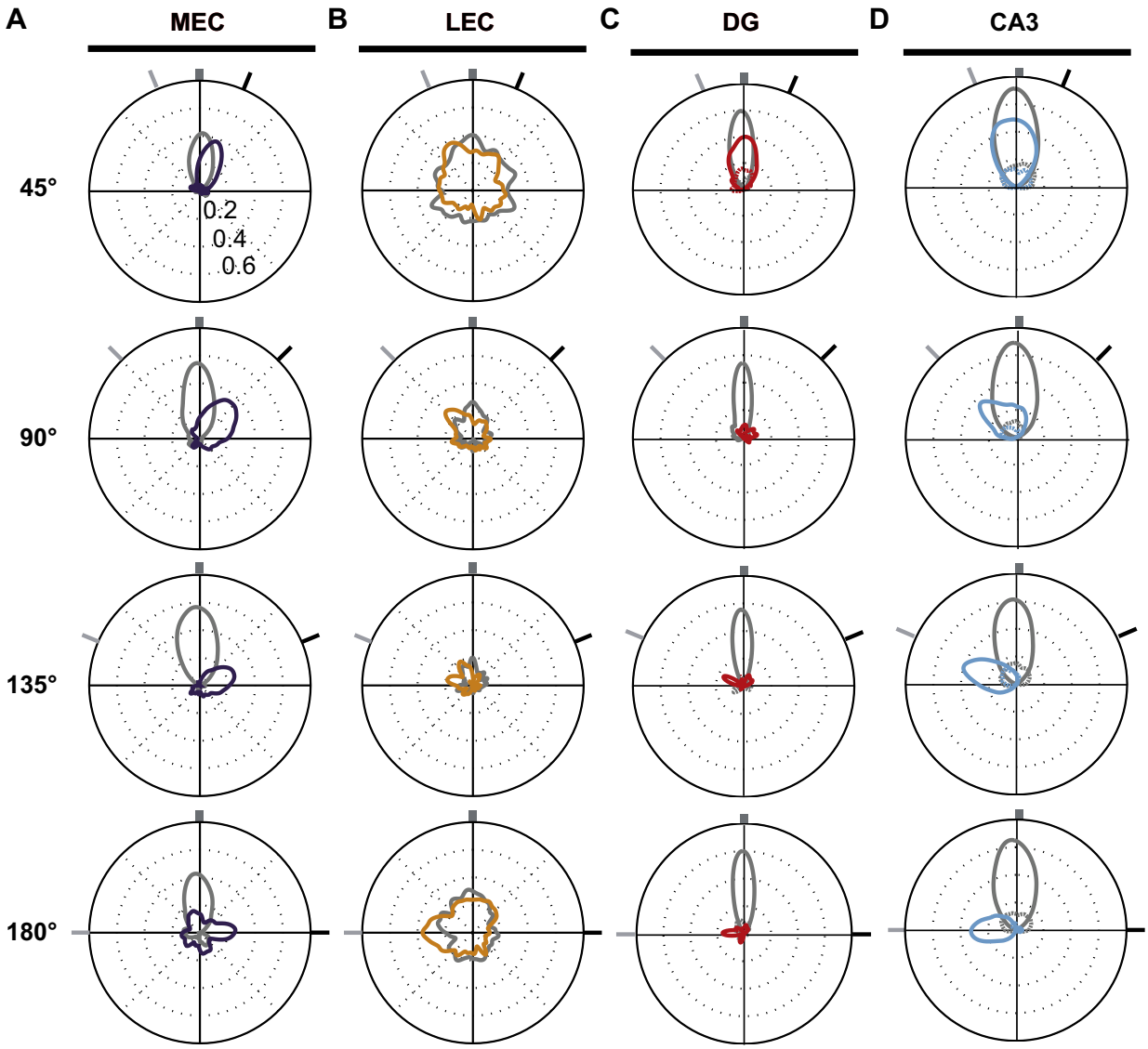


**Fig. 6.** Responses of the MEC, LEC, DG, and CA3 populations to the double rotation. Each polar plot denotes the correlation between the population representations of two standard sessions (gray plots) or between a standard and a mismatch session (colored plots). The correlation value is plotted along the radial dimension and the angular dimension indicates the amount that the population vectors were rotated relative to each other. The dark tick marks at the outer ring indicate the rotation extent of the global cues and the light tick marks indicate the rotation extent of the local cues, as in Fig. 5C. High population correlations are indicated by well-formed tuning curves with larger peak correlations; low population correlations are indicated by poorly formed tuning curves with smaller peak correlations. See original reports for more details. (A) MEC population correlations degraded gracefully with increasing mismatch angles and were controlled by the global (G) cues. From Neunuebel et al. (2013). (B) LEC population correlations were poorly tuned in all standard-standard and standard-mismatch comparisons, but the peak correlations were controlled by the local (L) cues. From Neunuebel et al. (2013). (C) DG population correlations were well-formed for the 45° mismatch, but became almost completely decorrelated with the larger mismatch sessions. The population of DG cells with significant spatial information is plotted. Modified from Supplementary Data in Neunuebel and Knierim (2014). (D) CA3 population correlations were well-formed for all mismatch angles and were controlled by the local (L) cues. The population of CA3 cells with significant spatial information is plotted. Modified from Supplementary Data in Neunuebel and Knierim (2014). (For interpretation of the references to colour in this figure legend, the reader is referred to the web version of this article.)

sions) (Fig. 6C). Detailed comparison of the change in the MEC and the change in the DG suggests that the DG changed more than the MEC (i.e., the peak correlation for DG compared to its standard-standard correlation was less than the same comparison for MEC). With mismatch angles >90°, the DG representations of the standard and mismatch session become highly decorrelated, even while the MEC representations maintained a smoothly decreasing correlation. A minority of DG cells did not remap the two environments, and these cells tended to be controlled by the local cues. Overall, this pattern resembles strongly the hypothetical Δinput–Δoutput curve from Fig. 2. With small Δinput, the Δoutput was greater than the Δinput. With larger Δinput, the Δoutput was almost maximal, as the DG representations of the standard and mismatch session were almost completely decorrelated.

### *3.4. CA3 performs pattern completion/error correction/generalization on its DG/EC inputs*

Lee, Yoganarasimha, Rao, and Knierim (2004) showed that the CA3 population maintained a relatively coherent representation of the standard environment in the mismatch sessions. As the mismatch angle increased, the correlation slowly degraded, similar to the MEC input. Whereas the graceful degradation in MEC may reflect an increasing shift of the spatial representations of MEC relative to the track (e.g., grid cell firing patterns may shift in the horizontal plane, causing some grid vertices to "fall off" the track and other to "climb on"; Neunuebel et al., 2013), the degradation in CA3 may result from a combination of such a shift as well as an increase in partial remapping of CA3 cells. Critically, in contrast

to the MEC, the CA3 representation was controlled by the local cues, and Neunuebel and Knierim (2014) independently verified this finding (Fig. 6D). Thus, armed with the information about how the MEC, LEC, and DG inputs change with the increasing mismatch amount, we can begin to measure the Δinput–Δoutput curve for CA3. The MEC maintains a high degree of correlation between the standard and mismatch sessions, but the representation is controlled by the global cues (Fig. 6A). Thus, the MEC representation cannot explain the local-cue-controlled, coherent representations retrieved by the CA3 network. The LEC has weakly correlated representations between all standard and mismatch sessions (Fig. 6B), and the DG has weakly correlated representations between standard sessions and mismatch sessions >45° (Fig. 6C). Since the only cues that CA3 receives about the local cues appear to come from these weakly correlated inputs, this provides strong evidence for pattern completion in CA3 (i.e., a large Δinput results in a smaller Δoutput).

Importantly, in this experiment we do not appear to explore the parameter space in which the Δinput is large enough to detect the pattern separation functions of the CA3 attractor (i.e., the rightward extreme of the sigmoid curve of Fig. 2). However, experiments from other laboratories have shown evidence that the CA3 representations are completely independent under more extreme conditions that would presumably generate a larger Δinput from EC, (Guzowski et al., 2004; Leutgeb, Leutgeb, Treves, Moser, & Moser, 2004; Vazdarjanova & Guzowski, 2004). Leutgeb et al. (2004) recorded the activity of CA3 and CA1 place cells as rats explored similar enclosures in the same location or in completely different rooms. Under these conditions, the CA3 representations of the different rooms were completely orthogonal to each other, whereas the CA1 representations maintained some degree of similarity that presumably reflected the common aspects of the two rooms. Vazdarjanova and Guzowski (2004) imaged immediate early gene activity when changes to an environment were small (individual environmental cues were altered) or large (the rat was moved to a new room). With the small manipulations, the CA3 ensemble representation changed less than the CA1 representation; conversely, with the large change to a new environment, the CA3 representation changed more than the CA1 representation. Taken together with our double rotation data, these experiments suggest that CA3 displays the sigmoidal Δinput–Δoutput relationship predicted by theory (Guzowski et al., 2004; McClelland & Goddard, 1996; Rolls & Treves, 1998).

### 3.5. CA1 representations reflect a (linear?) combination of CA3 and EC inputs

Lee et al. (2004) demonstrated that CA1 populations created a split representation in the mismatch sessions, whereas CA3 simultaneously produced a more coherent representation controlled by the local cues. Some CA1 place fields rotated with the local cues and a similar number rotated with the global cues (some place fields even split in half, with one subfield rotating with the local cues and the other with the global cues). Like CA3, other CA1 cells showed a remapping response, either losing their firing fields or gaining a field.

Because the major input to CA1 is from CA3, the CA1 result seems counterintuitive. If the CA3 network goes through all the trouble of completing the input pattern of the altered environment, why does CA1 "ignore" this CA3 input and instead send the "corrupted" signal to the rest of the brain? It is important to realize that different parts of the transverse axis of CA1 receive input from different parts of the CA3 transverse axis as well as direct inputs from layer III of the EC. Proximal CA1 receives input from distal CA3 and from MEC, whereas distal CA1 receives input from proximal CA3 and LEC (Witter & Amaral, 2004; Witter, Wouterlood, Naber, & Van Haeften, 2000). The recordings from Lee et al. (2004) were primarily from proximal CA1 and from distal CA3. Thus, we can explain the split representation of CA1 by these anatomical projection patterns (Fig. 7). Proximal CA1 receives a local-cue-driven representation from distal CA3 and a global-cue-driven representation from MEC. Lacking a strong recurrent collateral system, it appears that CA1 performs a linear operation on its inputs: the inputs convey separate local and global representations, so the CA1 output forms a split representation that mimics the dual nature of its inputs. This split representation may reflect the comparator function often ascribed to CA1, that it compares the EC representation about the current state of the world with the mnemonic representations stored in CA3 of expected events predicted by the current inputs (Hasselmo, 2005; Levy, 1996; Lisman & Otmakhova, 2001; Vinogradova, 2001). Thus, the competition between pattern separation and pattern completion in the DG-CA3 processing loop retrieves from CA3 the most likely stored representation based on the current input, and this representation is then compared to the current input in CA1. Analogously, we would expect that distal CA1 would show responses that reflect a relatively linear combination of its inputs from proximal CA3 and LEC. Although such a comparator function was not explicitly demonstrated in our analyses, a finer-grained analysis (perhaps segregating EC-related firing from CA3-related firing based on variables such as theta phase or firing coherence at beta, low gamma, and high gamma frequency bands; Bieri, Bobbitt, & Colgin, 2014; Colgin et al., 2009; Hasselmo, Bodelon, & Wyble, 2002; Igarashi, Lu, Colgin, Moser, & Moser, 2014) might reveal intriguing neural dynamics between the CA1 local and global representations that could underlie such a comparison.

Fig. 8 summarizes the relationship between the LEC, MEC, and DG spatial input patterns to CA3 and the responses of these cell populations to the double rotation experiment. For clarity of presentation, the CA3 population activity on the circular track is depicted as a ring attractor, although the activity of place cells is more accurately modeled as a 2-dimensional sheet attractor (Knierim & Zhang, 2012; Samsonovich & McNaughton, 1997; Zhang, 1996). The cyan circles represent cells with place fields at the corresponding locations on the track. The diameters of the circles indicate the current firing rate of each cell, with larger diameters indicating higher firing rates. The green lines indicate excitatory connections among cells with neighboring place fields and the dashed black lines indicate inhibitory connections to all other cells. Although the excitatory and inhibitory connections are shown only for cells at the top of the ring, all cells have this connectivity pattern, resulting in a continuous ring attractor in which every location on the track is a stable state. With appropriate weights, a single bump of activity will form on this ring even in the absence of external inputs. When external inputs are added to the network, the location of the activity bump can be set by these inputs. The colored rings below demonstrate the activity levels of cells in the LEC, MEC, and DG inputs to CA3 when the rat is located at the north location on the track (left column). It is important to note that these rings indicate the activity of *cells* that represent locations on the track; they do not represent the *place fields* on the track. A topography of projections is assumed, such that cells that represent a certain location on the track project to cells in CA3 that represent the same location. The orange LEC ring shows a noisy representation with only a weak bias for higher activity at the north representation in the standard session. The purple MEC ring shows a well-formed spatial representation at the current location of the rat, from grid cells and other spatially modulated cells. The red DG ring also shows a well-formed spatial representation of the current location of the rat from DG place cells. In the familiar, standard environment, these 3 representations provide a coherent input to CA3 that drives the CA3 attractor

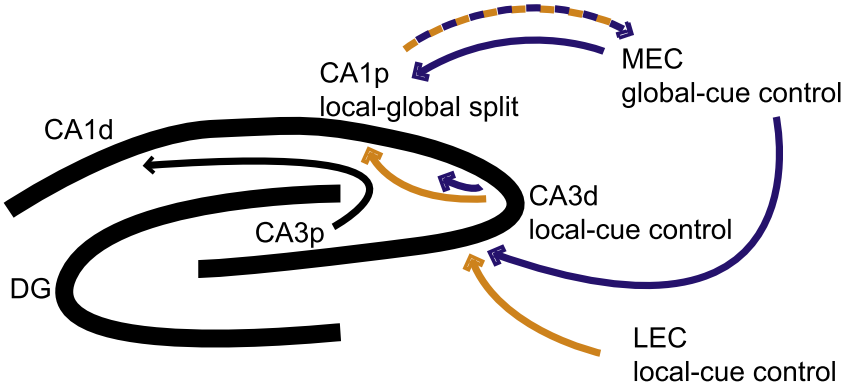


**Fig. 7.** Proximal CA1 (CA1p) receives input from the MEC that is controlled by the global cues. It also receives input from distal CA3 (CA3d) that is controlled primarily by local cues. The CA1 output back to the deep layers of MEC is an apparent linear split representation of the conflicting local–global inputs it receives from its afferent inputs. That is, CA1 receives conflicting reference frame signals from its inputs, and its outputs faithfully reflect this conflict. Adapted from Neunuebel et al. (2013).

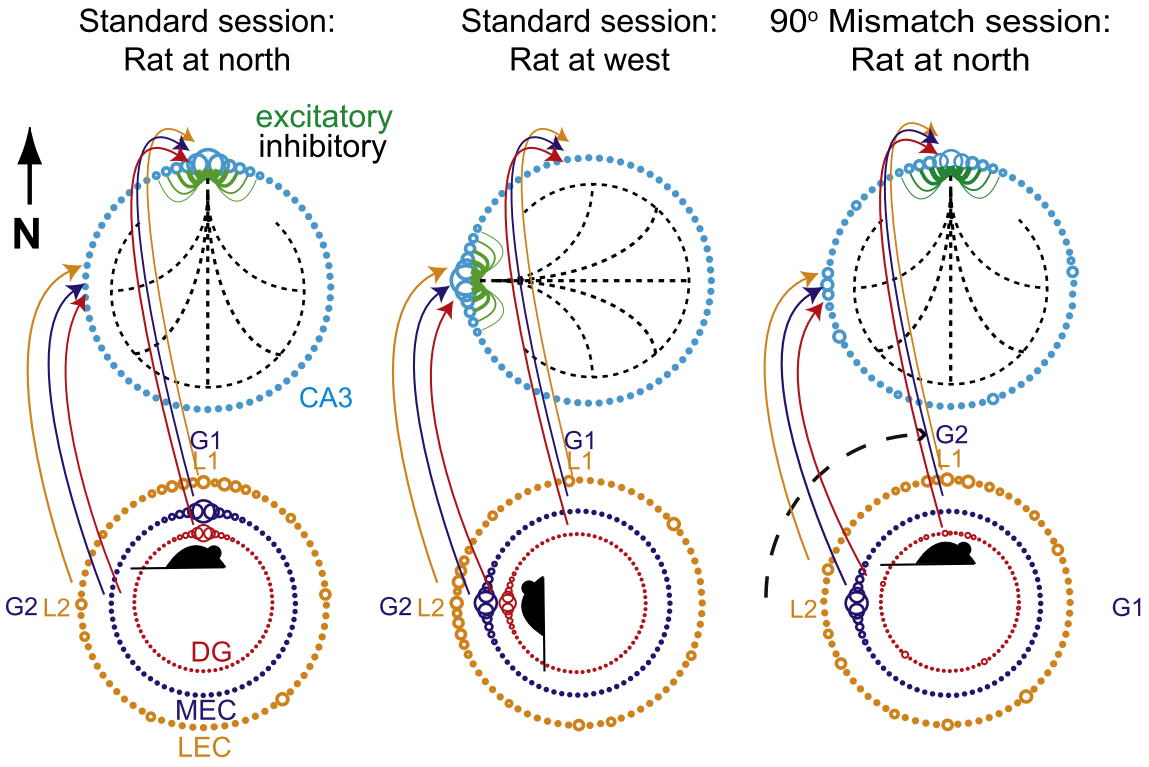


**Fig. 8.** Putative attractor dynamics of CA3. CA3 population activity is represented schematically as a bump in a continuous ring attractor. Excitatory connections are shown in green and inhibitory connections are in black (dashed lines). Inputs from DG, MEC, and LEC are indicated as input rings of activity. In the standard session (left column), the active inputs when the rat is at the north location of the track drive the CA3 activity bump at the north location of the ring. G1 and G2 refer to the locations of two global cues that control MEC activity, and L1 and L2 refer to the locations of two local cues that control LEC activity. When the rat is on the west location of the track (middle column), the corresponding cells controlled by the G2 and L2 cues cause the CA3 activity bump at the west location of the attractor ring. The right column shows the active cells during a mismatch session when the rat is back at the north location. For clarity of illustration, we show a 90° CW rotation of the global cues alone, which, in the absence of any other reference frame, is equivalent to the 90° mismatch of the double rotation. When the global cues are rotated 90° CW, the DG remaps and the LEC continues to fire in a weak spatial representation controlled by the local cues (L1). However, because the G2 global cues have been rotated to the north, the MEC cells that formerly encoded the west location defined by the G2 global cues are now active when the rat is at north. The CA3 attractor dynamics cause a relatively coherent activity bump to form at the local-cue-predicted location.

bump to form at the north location. Similarly, when the rat is at the west location (middle column), the corresponding cells fire as input to CA3, causing the attractor bump to form at the west location.

The right column illustrates the 90° mismatch condition, as two global cues (indicated G1 and G2) rotate CW. (For clarity of illustration, the global cues are rotated 90° CW and the local cues remain stationary. In the absence of any other polarizing cues, this situation mimics precisely the double rotation condition in terms of the local–global mismatch.) When the rat is placed on the track at the north location, it perceives the local cues at that same location. Thus, the LEC cells will fire as before. However, because the MEC representation follows the global cues, the cells that were active at the north location in the standard session are now silent,

as they will fire only when the rat travels to the east location (where G1 is now visible). The MEC cells active at the initial G2 location (west in the standard session; middle column) are active instead, sending excitatory drive to the west location of the CA3 ring. Finally, the DG representation has almost entirely remapped (pattern separation), with a weak bias for the cells at the north location to fire. Other DG cells that encode random locations on the track are also active, indicating the global remapping that occurs in the DG.

Given these inputs, the attractor dynamics in CA3 determine how the CA3 place cells fire in the mismatch session. The data clearly indicate that CA3 is controlled by the local cues. Thus, the combined LEC and DG input apparently form the "seed" that biases the attractor bump (i.e., the active cells in Fig. 8) to fire in the local-cue-predicted location. Although the MEC provides a strong input for CA3 cells that represent the global cues (G2) to fire, the inhibition from the attractor bump appears to prevent strong activity at that location of the ring. (The CA3 data show that there are a small number of CA3 cells controlled by the global cues, suggesting that the strong external drive can overcome the attractor dynamics to some degree (Lee et al., 2004; Neunuebel & Knierim, 2014)). Other active cells outside the bump can generate alterations in the attractor dynamics, such as the formation of spurious attractor states (Knierim & Zhang, 2012), as the result of the conflict between the external inputs. Thus, given the altered input patterns of it inputs, we see that the CA3 attractor dynamics allow the input "errors" to be partially corrected and a single, coherent output representation to form. When the rat is at the north, the inputs to the north CA3 cells are severely weakened and degraded by the absence of the drive from MEC and DG. However, the ability of the network to form a strong activity bump at this location, given the weak inputs, can be considered a demonstration of pattern completion.

It is important to note that these diagrams illustrate only the sets of active cells that represent the standard environment. Not depicted are other DG and CA3 cells that were silent in the standard session but that became active in the mismatch session. In cases of "global remapping," completely different ensembles of neurons (active sets) are activated as the result of large environmental changes (Kubie & Ranck, 1983). The different active sets correspond to activity on different "charts," to use the terminology of Samsonovich and McNaughton (1997). Such global remapping in CA3, such as that produced by bringing the rat to a completely different environment (Colgin et al., 2010; Leutgeb et al., 2005; but see Knierim, 2003), would show the pattern separation properties of CA3 and could be depicted by adding a new attractor ring to the diagram that illustrates a new CA3 "chart," with its own activity bump (Samsonovich & McNaughton, 1997).

### 3.6. Relationship between DG and CA3

A number of further considerations can be appreciated from these illustrations. Pattern separation is often considered to be an operation that occurs during memory storage and pattern completion to be a process that occurs during memory retrieval. Although this can be a conceptually useful distinction, it is unlikely to completely hold true when discussing the neurophysiological mechanisms underlying these processes. According to Fig. 2A, the DG automatically orthogonalizes 2 different input patterns, regardless of whether these input patterns are new memories to be stored or retrieval cues to reinstate previously stored memories. It is the attractor dynamics of CA3 that determines whether a new memory pattern will be stored or whether a previously stored pattern will be retrieved. When CA3 is presented with input cues from EC in a novel environment, the representation is sparsified in the DG and the powerful mossy fiber inputs from DG to CA3 impose a pattern of activity on CA3 that becomes associated with the same EC cues that drove DG (Treves & Rolls, 1992). The next time that the animal receives the same input (e.g., when it returns to a particular location in an environment), the DG cells fire again and are presumably part of the inputs to CA3 that drive the reactivation of the same CA3 place cells as before. Thus, the DG is active during both storage (setting up the initial attractor representation in CA3) and retrieval (reactivating this attractor).

What occurs when the animal enters a completely different environment? The EC inputs are presumably very different in the new environment ($\Delta$input is high), and the DG imposes a completely novel pattern of activity on the CA3 network, creating a new attractor basin in CA3 that is associated with the EC inputs. The interesting dynamics occur when the new environment is only partly different. If the change to the EC inputs is small, the EC input will place the activity pattern of CA3 within the basin of attraction of the initial pattern. The DG input pattern will be less similar to the initial representation, due to the pattern separation, but if this does not drive the CA3 pattern far enough away from the attractor basin, then the system will retrieve a pattern similar to the initial pattern (pattern completion/generalization). As the EC input changes even further, the DG will continue to drive the CA3 pattern away from the original pattern, but the EC will drive it to fire within the basin. Eventually, the combined input of both EC and DG will cause CA3 to fire in a pattern outside the initial attractor, and this will then cause a new attractor basin to emerge. Under this scenario, the DG is always providing an input to drive CA3 away from a stored attractor basin (driving CA3 toward pattern separation). Whether CA3 actually performs pattern completion or pattern separation depends on the relative balance of EC inputs and DG inputs, as well as on the strength of the attractors stored within the CA3 network and other modulatory inputs that may alter the relative weights of the DG/EC inputs. These ideas might be explicitly tested with optogenetics or other techniques that could selectively enhance/suppress either the EC or DG inputs to CA3 and thereby causally tip the balance in favor of pattern separation or pattern completion in ambiguous environments.

## 4. Final comments and caveats

With this review we hope to have demonstrated how a series of experimental studies from our laboratory over the past decade have provided direct, physiological evidence in favor of classic models of hippocampal computation and its relationship to memory. We have taken the approach from the computational literature that the concepts of pattern separation and pattern completion can only be studied directly in terms of input–output transformations of neural representations (McClelland & Goddard, 1996; O'Reilly and McClelland, 1994; Santoro, 2013; Treves & Rolls, 1994). Thus, we have investigated the responses of 6 specific processing stages in the hippocampal circuit (anterior thalamus, LEC, MEC, DG, CA3, and CA1) to a manipulation designed to introduce graded changes to the hippocampal inputs. By measuring the correlations between the representations of the standard and cue-mismatch sessions, we provided evidence that conforms well to the models' predictions that the DG performs pattern separation and that the CA3 contains attractor dynamics that can support pattern completion.

A number of caveats are in order, however. The data presented in this review capture the essence of the results, but the entire picture is much more complex, and the interested reader is directed to the original research reports to find further details. Moreover, the hippocampal anatomy is more complex than that described here. Although the MEC and LEC are the major inputs into the hippocampus, there are other inputs (such as from the septum, perirhinal cortex, and brainstem) that we have not accounted for in our

recordings or interpretation. A thorough understanding of the computational functions of each subregion will require more detailed knowledge about all of the inputs and outputs of the hippocampus. Similarly, the population analyses reviewed here combine the many different types of neural responses found in the hippocampal formation, recorded over multiple sessions, into a single, population vector code (e.g., place cells, object cells, silent cells in the hippocampus; grid cells, head direction cells, boundary cells, unclassified cells in the MEC). It remains to be determined how the different functional cell types may play distinct roles in these mnemonic processes. A particularly critical question concerns the role of adult neurogenesis in the functions of the DG (Akers et al., 2014; Frankland, Kohler, & Josselyn, 2013; Kesner et al., 2014; Nakashiba et al., 2012). The DG data presented here come from all cells in the DG that met certain spatial information criteria. Although these criteria presumably excluded interneurons, it is not clear how many cells were fully mature granule cells, immature (newborn) granule cells, or mossy cells of the hilus region (Neunuebel & Knierim, 2012). Understanding the functions of these different excitatory cell types will be crucial for a complete understanding of DG function.

Furthermore, there are anatomical and functional differences along the hippocampal transverse axis within CA3 and within CA1 that warrant further investigation (Henriksen et al., 2010; Nakamura, Flasbeck, Maingret, Kitsukawa, & Sauvage, 2013; Witter et al., 2000). For example, in contrast to distal and intermediate CA3, which show the pattern completion phenomena described above, proximal CA3 (within the blades of the DG) responds to the double rotation similarly to the DG (i.e., it appears to perform pattern separation) (Lee, Wang, Deshmukh, & Knierim, 2015). This functional differentiation along the CA3 transverse axis is consistent with the increasing density of recurrent collaterals from proximal to distal CA3 (see also Lu, Igarashi, Witter, Moser, & Moser, 2015). We also need to know how the CA2 region, which has been mostly ignored in the literature until recently, fits into the picture (Caruana, Alexander, & Dudek, 2012; Chevaleyre & Siegelbaum, 2010; Hitti & Siegelbaum, 2014; Jones & McHugh, 2011; Mankin, Diehl, Sparks, Leutgeb, & Leutgeb, 2015). In experiments demonstrating pattern completion (Lee et al., 2015) and pattern separation (Lu et al., 2015), CA2 appears to act like the distal CA3 region. Our laboratory is currently investigating how proximal CA1 differs from distal CA1 in the double rotation experiment.

Finally, although we have used the spatially selective firing of hippocampal neurons to test the specific predictions of the computational theories, these experiments have not addressed specifically how these neural computations can underlie memory performance. Relating the neurophysiology to behavioral tests of pattern separation and pattern completion (Rolls & Kesner, 2006; Yassa & Stark, 2011) will help close the loop between theory and experiment and provide key insights into the neural circuit mechanisms underlying the mnemonic functions of the hippocampus. At the moment we can only speculate how the different hippocampal regions would respond in a hippocampus-dependent memory task, and how these responses would correlate with the animal's behavioral performance. Because the double rotation task does not have a memory component, it is difficult to make any direct correspondence from these neural response patterns to memory performance. However, one might speculate on how these results would predict hippocampal responses in an unrelated memory task. For example, seeing a familiar face at a distance in an unfamiliar context can often lead to confusion about the identity of that person. If there is a strong attractor representation in CA3, the degraded input from the distant face (presumably encoded by LEC) may be strong enough to activate the attractor, not only recalling the identity of the person but also the spatiotemporal context (presumably encoded by the MEC) in which one last met that person. Reactivating neocortical representations via CA1 output to construct a full recollection of the event would constitute an episodic memory. However, upon greeting the familiar-looking person, one may realize that this is a complete stranger when they do not return the greeting. Under these conditions, the pattern separation mechanisms of the DG may impose a new attractor in the CA3 region to create a completely distinct representation of the stranger, such that in the future one does not repeat the error. Even in situations in which the memory retrieval was correct, one still would wish to remember the original episode in which the person was previously encountered as well as storing a new memory of the current meeting. Perhaps this dual function explains why the CA3 region displays a topographical organization along its transverse axis, in which the proximal part of CA3 is biased toward pattern separation (to form a new, distinct memory of the current episode) whereas the distal part of CA3 is simultaneously biased toward pattern completion (to retrieve the memory of the prior episode). Experiments utilizing high-resolution imaging with human subjects might be able to test these ideas and bridge the neurophysiological results from rodents with the neuropsychological literature on human episodic memory, with both approaches interpreted in the framework of memory processing from the computational literature.

## Acknowledgments

We thank I. Lee, D. Yoganarasimha, F. Savelli, and G. Rao for help in data collection for some of the figures shown in this manuscript. The experiments reviewed here were supported by Public Health Service grants NS039456 and MH094146 and by the Johns Hopkins University Brain Sciences Institute. The funding agency had no role in the design, data collection, analysis, or writing of the paper.

## References

Akers, K. G., Martinez-Canabal, A., Restivo, L., Yiu, A. P., De Cristofaro, A., Hsiang, H. L., ... Frankland, P. W. (2014). Hippocampal neurogenesis regulates forgetting during adulthood and infancy. *Science, 344*, 598–602.

Bakker, A., Kirwan, C. B., Miller, M., & Stark, C. E. (2008). Pattern separation in the human hippocampal CA3 and dentate gyrus. *Science, 319*, 1640–1642.

Bieri, K. W., Bobbitt, K. N., & Colgin, L. L. (2014). Slow and fast gamma rhythms coordinate different spatial coding modes in hippocampal place cells. *Neuron, 82*, 670–681.

Blair, H. T. (1996). A thalamocortical circuit for computing directional heading in the rat. *Advances in Neural Information Processing Systems, 8*, 152–158.

Bostock, E., Muller, R. U., & Kubie, J. L. (1991). Experience-dependent modifications of hippocampal place cell firing. *Hippocampus, 1*, 193–205.

Brun, V. H., Solstad, T., Kjelstrup, K. B., Fyhn, M., Witter, M. P., Moser, E. I., & Moser, M. B. (2008). Progressive increase in grid scale from dorsal to ventral medial entorhinal cortex. *Hippocampus, 18*, 1200–1212.

Caruana, D. A., Alexander, G. M., & Dudek, S. M. (2012). New insights into the regulation of synaptic plasticity from an unexpected place: Hippocampal area CA2. *Learning & Memory, 19*, 391–400.

Chevaleyre, V., & Siegelbaum, S. A. (2010). Strong CA2 pyramidal neuron synapses define a powerful disynaptic cortico-hippocampal loop. *Neuron, 66*, 560–572.

Colgin, L. L., Denninger, T., Fyhn, M., Hafting, T., Bonnevie, T., Jensen, O., ... Moser, E. I. (2009). Frequency of gamma oscillations routes flow of information in the hippocampus. *Nature, 462*, 353–357.

Colgin, L. L., Leutgeb, S., Jezek, K., Leutgeb, J. K., Moser, E. I., McNaughton, B. L., & Moser, M.-B. (2010). Attractor-map versus autoassociation based attractor dynamics in the hippocampal network. *Journal of Neurophysiology, 104*, 35–50.

Deshmukh, S. S., & Knierim, J. J. (2011). Representation of non-spatial and spatial information in the lateral entorhinal cortex. *Frontiers in Behavioral Neuroscience, 5*, 69. http://dx.doi.org/10.3389/fnbeh.2011.00069.

Deshmukh, S. S., Yoganarasimha, D., Voicu, H., & Knierim, J. J. (2010). Theta modulation in the medial and the lateral entorhinal cortex. *Journal of Neurophysiology, 104*, 994–1006.

Frankland, P. W., Kohler, S., & Josselyn, S. A. (2013). Hippocampal neurogenesis and forgetting. *Trends in Neurosciences, 36*, 497–503.

Gilbert, P. E., Kesner, R. P., & Lee, I. (2001). Dissociating hippocampal subregions: Double dissociation between dentate gyrus and CA1. *Hippocampus, 11*, 626–636.

Guzowski, J. F., Knierim, J. J., & Moser, E. I. (2004). Ensemble dynamics of hippocampal regions CA3 and CA1. *Neuron, 44*, 581–584.

Hafting, T., Fyhn, M., Bonnevie, T., Moser, M. B., & Moser, E. I. (2008). Hippocampus-independent phase precession in entorhinal grid cells. *Nature, 453*, 1248–1252.
Hafting, T., Fyhn, M., Molden, S., Moser, M. B., & Moser, E. I. (2005). Microstructure of a spatial map in the entorhinal cortex. *Nature, 436*, 801–806.
Hargreaves, E. L., Rao, G., Lee, I., & Knierim, J. J. (2005). Major dissociation between medial and lateral entorhinal input to dorsal hippocampus. *Science, 308*, 1792–1794.
Hargreaves, E. L., Yoganarasimha, D., & Knierim, J. J. (2007). Cohesiveness of spatial and directional representations recorded from neural ensembles in the anterior thalamus, parasubiculum, medial entorhinal cortex, and hippocampus. *Hippocampus, 17*, 826–841.
Hasselmo, M. E. (2005). The role of hippocampal regions CA3 and CA1 in matching entorhinal input with retrieval of associations between objects and context: Theoretical comment on Lee et al. (2005). *Behavioral Neuroscience*, 119, 342–345.
Hasselmo, M. E., Bodelon, C., & Wyble, B. P. (2002). A proposed function for hippocampal theta rhythm: Separate phases of encoding and retrieval enhance reversal of prior learning. *Neural Computation, 14*, 793–817.
Henriksen, E. J., Colgin, L. L., Barnes, C. A., Witter, M. P., Moser, M. B., & Moser, E. I. (2010). Spatial representation along the proximodistal axis of CA1. *Neuron, 68*, 127–137.
Hitti, F. L., & Siegelbaum, S. A. (2014). The hippocampal CA2 region is essential for social memory. *Nature, 508*, 88–92.
Igarashi, K. M., Lu, L., Colgin, L. L., Moser, M.-B., & Moser, E. I. (2014). Coordination of entorhinal–hippocampal ensemble activity during associative learning. *Nature, 510*, 143–147.
Jones, M. W., & McHugh, T. J. (2011). Updating hippocampal representations: CA2 joins the circuit. *Trends in Neurosciences, 34*, 526–535.
Kesner, R. P., Gilbert, P. E., & Wallenstein, G. V. (2000). Testing neural network models of memory with behavioral experiments. *Current Opinion in Neurobiology, 10*, 260–265.
Kesner, R. P., Hui, X., Sommer, T., Wright, C., Barrera, V. R., & Fanselow, M. S. (2014). The role of postnatal neurogenesis in supporting remote memory and spatial metric processing. *Hippocampus, 24*, 1663–1671.
Knierim, J. J. (2002). Dynamic interactions between local surface cues, distal landmarks, and intrinsic circuitry in hippocampal place cells. *Journal of Neuroscience, 22*, 6254–6264.
Knierim, J. J. (2003). Hippocampal remapping: Implications for spatial learning and navigation. In K. J. Jeffery (Ed.), *The neurobiology of spatial behaviour* (pp. 226–239). Oxford: Oxford University Press.
Knierim, J. J., Kudrimoti, H. S., & McNaughton, B. L. (1995). Place cells, head direction cells, and the learning of landmark stability. *The Journal of Neuroscience, 15*, 1648–1659.
Knierim, J. J., Kudrimoti, H. S., & McNaughton, B. L. (1998). Interactions between idiothetic cues and external landmarks in the control of place cells and head direction cells. *Journal of Neurophysiology, 80*, 425–446.
Knierim, J. J., Neunuebel, J. P., & Deshmukh, S. S. (2013). Functional correlates of the lateral and medial entorhinal cortex: Objects, path integration and local–global reference frames. *Philosophical Transactions of the Royal Society of London. Series B, Biological Sciences, 369*, 20130369.
Knierim, J. J., & Zhang, K. (2012). Attractor dynamics of spatially correlated neural activity in the limbic system. *Annual Review of Neuroscience, 35*, 267–285.
Kubie, J. L., & Ranck, J. B. Jr., (1983). Sensory-behavioral correlates in individual hippocampus neurons in three situations: Space and context. In W. Seifert (Ed.), *Neurobiology of the Hippocampus* (pp. 433–447). London: Academic Press.
Lee, H., Wang, C., Deshmukh, S. S., & Knierim, J. J. (2015). Neural population evidence of functional heterogeneity along the CA3 transverse axis: Pattern completion versus pattern separation. *Neuron, 87*, 1093–1105.
Lee, I., Yoganarasimha, D., Rao, G., & Knierim, J. J. (2004). Comparison of population coherence of place cells in hippocampal subfields CA1 and CA3. *Nature, 430*, 456–459.
Leutgeb, S., Leutgeb, J. K., Barnes, C. A., Moser, E. I., McNaughton, B. L., & Moser, M.-B. (2005). Independent codes for spatial and episodic memory in hippocampal neuronal ensembles. *Science, 309*, 619–623.
Leutgeb, S., Leutgeb, J. K., Treves, A., Moser, M. B., & Moser, E. I. (2004). Distinct ensemble codes in hippocampal areas CA3 and CA1. *Science, 305*, 1295–1298.
Levy, W. B. (1996). A sequence predicting CA3 is a flexible associator that learns and uses context to solve hippocampal-like tasks. *Hippocampus, 6*, 579–590.
Lisman, J. E., & Otmakhova, N. A. (2001). Storage, recall, and novelty detection of sequences by the hippocampus: Elaborating on the SOCRATIC model to account for normal and aberrant effects of dopamine. *Hippocampus, 11*, 551–568.
Lu, L., Igarashi, K. M., Witter, M. P., Moser, E. I., & Moser, M.-B. (2015). Topography of place maps along the CA3-to-CA2 axis of the hippocampus. *Neuron, 87*, 1078–1092.
Mankin, E. A., Diehl, G. W., Sparks, F. T., Leutgeb, S., & Leutgeb, J. K. (2015). Hippocampal CA2 activity patterns change over time to a larger extent than between spatial contexts. *Neuron, 85*, 190–201.
Marr, D. (1969). A theory of cerebellar cortex. *The Journal of Physiology, 202*, 437–470.
Marr, D. (1971). Simple memory: A theory for archicortex. *Philosophical Transactions of the Royal Society of London. Series B: Biological Sciences, 262*, 23–81.
McClelland, J. L., & Goddard, N. H. (1996). Considerations arising from a complementary learning systems perspective on hippocampus and neocortex. *Hippocampus, 6*, 654–665.
McHugh, T. J., Jones, M. W., Quinn, J. J., Balthasar, N., Coppari, R., Elmquist, J. K., ... Tonegawa, S. (2007). Dentate gyrus NMDA receptors mediate rapid pattern separation in the hippocampal network. *Science, 317*, 94–99.
McNaughton, B. L., & Morris, R. G. M. (1987). Hippocampal synaptic enhancement and information storage within a distributed memory system. *Trends in Neuroscience, 10*, 408–415.
McNaughton, B. L., & Nadel, L. (1990). Hebb–Marr networks and the neurobiological representation of action in space. In M. A. Gluck & D. E. Rumelhart (Eds.), *Neuroscience and connectionist theory* (pp. 1–63). Hillsdale, N.J: Erlbaum.
Monaco, J. D., Rao, G., Roth, E. D., & Knierim, J. J. (2014). Attentive scanning behavior drives one-trial potentiation of hippocampal place fields. *Nature Neuroscience, 17*, 725–731.
Myers, C. E., & Scharfman, H. E. (2009). A role for hilar cells in pattern separation in the dentate gyrus: A computational approach. *Hippocampus, 19*, 321–337.
Myers, C. E., & Scharfman, H. E. (2011). Pattern separation in the dentate gyrus: A role for the CA3 backprojection. *Hippocampus, 21*, 1190–1215.
Nakamura, N. H., Flasbeck, V., Maingret, N., Kitsukawa, T., & Sauvage, M. M. (2013). Proximodistal segregation of nonspatial information in CA3: Preferential recruitment of a proximal CA3-distal CA1 network in nonspatial recognition memory. *The Journal of Neuroscience, 33*, 11506–11514.
Nakashiba, T., Cushman, J. D., Pelkey, K. A., Renaudineau, S., Buhl, D. L., McHugh, T. J., ... Tonegawa, S. (2012). Young dentate granule cells mediate pattern separation, whereas old granule cells facilitate pattern completion. *Cell, 149*, 188–201.
Neunuebel, J. P., & Knierim, J. J. (2012). Spatial firing correlates of physiologically distinct cell types of the rat dentate gyrus. *The Journal of Neuroscience, 32*, 3848–3858.
Neunuebel, J. P., & Knierim, J. J. (2014). CA3 retrieves coherent representations from degraded input: Direct evidence for CA3 pattern completion and dentate gyrus pattern separation. *Neuron, 81*, 416–427.
Neunuebel, J. P., Yoganarasimha, D., Rao, G., & Knierim, J. J. (2013). Conflicts between local and global spatial frameworks dissociate neural representations of the lateral and medial entorhinal cortex. *The Journal of Neuroscience, 33*, 9246–9258.
O'Reilly, R. C., & McClelland, J. L. (1994). Hippocampal conjunctive encoding, storage, and recall: Avoiding a trade-off. *Hippocampus, 4*, 661–682.
Ranck, J. B. Jr., (1973). Studies on single neurons in dorsal hippocampal formation and septum in unrestrained rats. I. Behavioral correlates and firing repertoires. *Experimental Neurology, 41*, 461–531.
Redish, A. D., Elga, A. N., & Touretzky, D. S. (1996). A coupled attractor model of the rodent head direction system. *Network: Computation in Neural System, 7*, 671–685.
Rolls, E. T., & Kesner, R. P. (2006). A computational theory of hippocampal function, and empirical tests of the theory. *Progress in Neurobiology, 79*, 1–48.
Rolls, E. T., & Treves, A. (1998). *Neural networks and brain function*. Oxford: Oxford University Press.
Samsonovich, A., & McNaughton, B. L. (1997). Path integration and cognitive mapping in a continuous attractor neural network model. *The Journal of Neuroscience, 17*, 5900–5920.
Santoro, A. (2013). Reassessing pattern separation in the dentate gyrus. *Frontiers in Behavioral Neuroscience, 7*, 96.
Sargolini, F., Fyhn, M., Hafting, T., McNaughton, B. L., Witter, M. P., Moser, M. B., & Moser, E. I. (2006). Conjunctive representation of position, direction, and velocity in entorhinal cortex. *Science, 312*, 758–762.
Savelli, F., Yoganarasimha, D., & Knierim, J. J. (2008). Influence of boundary removal on the spatial representations of the medial entorhinal cortex. *Hippocampus, 18*, 1270–1282.
Shapiro, M. L., Tanila, H., & Eichenbaum, H. (1997). Cues that hippocampal place cells encode: Dynamic and hierarchical representation of local and distal stimuli. *Hippocampus, 7*, 624–642.
Skaggs, W. E., Knierim, J. J., Kudrimoti, H. S., & McNaughton, B. L. (1995). A model of the neural basis of the rat's sense of direction. *Advances in Neural Information Processing Systems, 7*, 173–180.
Solstad, T., Boccara, C. N., Kropff, E., Moser, M. B., & Moser, E. I. (2008). Representation of geometric borders in the entorhinal cortex. *Science, 322*, 1865–1868.
Song, P., & Wang, X. J. (2005). Angular path integration by moving "hill of activity": A spiking neuron model without recurrent excitation of the head-direction system. *The Journal of Neuroscience, 25*, 1002–1014.
Stewart, M., Quirk, G. J., Barry, M., & Fox, S. E. (1992). Firing relations of medial entorhinal neurons to the hippocampal theta rhythm in urethane anesthetized and walking rats. *Experimental Brain Research, 90*, 21–28.
Taube, J. S., Muller, R. U., & Ranck, J. B. Jr., (1990). Head-direction cells recorded from the postsubiculum in freely moving rats. II. Effects of environmental manipulations. *The Journal of Neuroscience, 10*, 436–447.
Treves, A., & Rolls, E. T. (1992). Computational constraints suggest the need for two distinct input systems to the hippocampal CA3 network. *Hippocampus, 2*, 189–199.
Treves, A., & Rolls, E. T. (1994). Computational analysis of the role of the hippocampus in memory. *Hippocampus, 4*, 374–391.
Vazdarjanova, A., & Guzowski, J. F. (2004). Differences in hippocampal neuronal population responses to modifications of an environmental context: Evidence for distinct, yet complementary, functions of CA3 and CA1 ensembles. *Journal of Neuroscience, 24*, 6489–6496.
Vinogradova, O. S. (2001). Hippocampus as comparator: Role of the two input and two output systems of the hippocampus in selection and registration of information. *Hippocampus, 11*, 578–598.
Witter, M. P., & Amaral, D. G. (2004). Hippocampal formation. In G. Paxinos (Ed.), *The rat nervous system* (3rd ed., pp. 635–704). Amsterdam: Elsevier.

Witter, M. P., Wouterlood, F. G., Naber, P. A., & Van Haeften, T. (2000). Anatomical organization of the parahippocampal–hippocampal network. *Annals of the New York Academy of Sciences, 911*, 1–24.

Yassa, M. A., & Stark, C. E. (2011). Pattern separation in the hippocampus. *Trends in Neurosciences, 34*, 515–525.

Yoganarasimha, D., Rao, G., & Knierim, J. J. (2011). Lateral entorhinal neurons are not spatially selective in cue-rich environments. *Hippocampus, 21*, 1363–1374.

Yoganarasimha, D., Yu, X., & Knierim, J. J. (2006). Head direction cell representations maintain internal coherence during conflicting proximal and distal cue rotations: Comparison with hippocampal place cells. *The Journal of Neuroscience, 26*, 622–631.

Zhang, K. (1996). Representation of spatial orientation by the intrinsic dynamics of the head-direction cell ensemble: A theory. *The Journal of Neuroscience, 16*, 2112–2126.

Zhang, S. J., Ye, J., Miao, C., Tsao, A., Cerniauskas, I., Ledergerber, D., ... Moser, E. I. (2013). Optogenetic dissection of entorhinal–hippocampal functional connectivity. *Science, 340*. http://dx.doi.org/10.1126/science.1232627.

Zugaro, M. B., Berthoz, A., & Wiener, S. I. (2001). Background, but not foreground, spatial cues are taken as references for head direction responses by rat anterodorsal thalamus neurons. *The Journal of Neuroscience, RC154*(1–5).